A Mathematical Model of Laser Drilling

Maturose Suchatawat*

Abstract

Laser drilling has been widely used for producing small diameter holes in hard-to-machine materials for decades. Of particular interest is laser drilling of cooling holes in aircraft turbine blades. In order to enhance the cooling efficiency, these cooling holes need to be produced to a high degree of accuracy and with least defects. In this paper, a mathematical model of laser drilling is developed. The model includes effects of the vapour pressure, exothermic energy and O_2 assist gas. The analysis is based on transient heat conduction in solid and liquid regions with appropriate boundary and initial conditions at the solid-liquid and liquid-vapour interfaces. Comparison with the experimental data is presented to validate the model. The developed model enables the prediction of the hole depth, hole profile and recast layer thickness. Effects of the laser peak power and assist gas pressure are also investigated

Keywords : Laser percussion drilling, Laser drilling model, Exothermic energy, Recast layer

Department of Mechanical Engineering, Faculty of Engineering, King Mongkut's Institute of Technology Ladkrabang, Bangkok 10520, Thailand.

* Corresponding author, E-mail: ksmaturo@kmitl.ac.th Received 9 July 2014, Accepted 3 November 2014

1. Introduction

Laser drilling has become a reliable option for a wide variety of industrial applications. This is due to its ability to precisely produce small, shaped holes in difficult-to-machine materials, with high processing speed and repeatability [1]. Laser drilling can be processed by means of single pulse, trepanning, percussion or helical drilling techniques [2]. Among these techniques, laser percussion drilling is considered as a prime candidate for applications where a large number of small precision holes with high aspect ratio are to be drilled.

In laser percussion drilling, a series of laser pulses is delivered to the same spot on the workpiece surface to produce a hole. If oxygen assist gas is used in the process, the molten metal may oxidise and adds exothermic energy to the laser beam-substrate interaction [3]. In some cases, plasma may be formed and traps part of the laser energy thereby resulting in beam scattering and hence less energy delivering to the workpiece [4]. Furthermore, the laser beam targeted to the hole bottom may reflect repeatedly along the cavity wall leading to the variation of the laser intensity inside the cavity [5].

Numerous laser percussion drilling models and simulation algorithms have been proposed to date [6-8]. However, most works either ignore the effects of the exothermic energy or disregard the temporal characteristics of the individual laser pulse which in fact have great influence on the drilling mechanisms. This indicates that the accuracy of the available models can be considerably improved by reducing the number of assumptions and by incorporating more related phenomena into the calculations.

In this paper, a mathematical model for multiple pulsed laser drilling is developed. The model accounts for the recoil pressure as well as the oxygen assist gas effects.

2. Mathematical model

A schematic diagram of the model is illustrated in Fig. 1(a).

A laser beam with intensity I_0 irradiates the substrate surface which is initially at temperature T_0. The solid substrate is then heated, melted and vaporized. Once the vapour is formed, it exerts recoil pressure on the molten liquid as it leaves the cavity, and pushes the melt away radially. The material removal therefore consists of two mechanisms; vaporization and melt ejection. Oxygen assist gas also plays some role in the process. The oxidation reaction between oxygen and metal provides the additional energy, called exothermic energy, to the laser beam-material interaction. The assist gas also enhances the melt ejection mechanism by adding more pressure to the recoil pressure. Moreover, the assist gas also promotes heat convection rate at the surface of the liquid layer. Fig. 1(b) illustrates variables defined in the model.

Following assumptions are made for the model:

1. The absorbed laser intensity distribution over the workpiece surface is assumed to be uniform.
2. Plasma generation is neglected in the model.
3. No interaction between laser beam and the vapour.
4. No laser power is absorbed by the ejected melt.
5. The generation of shock waves is ignored.
6. The changes in surface absorptivity, melting point, and boiling point due to oxide layer formed are neglected.
7. Not all of the metal oxidises with O_2 assist gas. The oxidation efficiency is introduced in the model.

2.1 Energy balance

Once the vaporization has started, the liquid-vapour and solid-liquid interfaces are formed, respectively, at

$$z = z_v(r,t) \tag{1}$$

$$z = z_m(r,t) \tag{2}$$

where r and t are radial distance and time. At the liquid-vapour interface, the Stefan equation can be written as:

$$\rho_l L_v \frac{\partial z_v}{\partial t} - k_l \frac{\partial T_l}{\partial z}\left[1+\left(\frac{\partial z_v}{\partial r}\right)^2\right] = I_{abs} + \rho_l H_{ox}\eta_{ox}\frac{\partial z_m}{\partial t} - h_g(T_{l0} - T_g) \tag{3}$$

where ρ_l, k_l and L_v are liquid density, thermal conductivity of liquid and latent heat of vaporization, I_{abs}, H_{ox}, η_{ox}, and h_g are absorbed laser intensity, enthalpy of oxidation, oxidation efficiency and heat transfer coefficient of assist gas, T_l, T_g and T_{l0} are temperature of the melt, assist gas, and melt surface, respectively.

The heat transfer coefficient, h_g ,can be determined from [9]

$$h_g = \frac{k_g}{2r_{v0}}\left(C_c\ \mathrm{Re}^{n_c}\ \mathrm{Pr}^{1/3}\right) \tag{4}$$

where r_{v0} is the radius of the liquid-vapour interface at the hole entrance, k_g, Re, and Pr are the thermal conductivity, Reynolds number, and Prandtl number of the assist gas, respectively, C_c and n_c are the constants for forced convection perpendicular to the liquid surface, and are taken to be 0.228 and 0.731 [10], respectively. The Reynolds number, Re, is expressed as:

$$\mathrm{Re} = \frac{\rho_g v_g 2r_{v0}}{\mu_g} \tag{5}$$

where ρ_g, v_g and μ_g are the density, flow velocity, and dynamic viscosity of the assist gas, respectively.

The Stefan equation for the solid-liquid interface can be written as.

$$\rho_s L_m \frac{\partial z_m}{\partial t} = \left(k_s \frac{\partial T_s}{\partial z} - k_l \frac{\partial T_l}{\partial z} \right) \left[1 + \left(\frac{\partial z_m}{\partial r} \right)^2 \right] \quad (6)$$

where ρ_s, k_s and T_s are density, thermal conductivity, and temperature of the solid, respectively.

At the symmetry axis, $\frac{\partial z_m}{\partial r} = 0$ and $\frac{\partial z_v}{\partial r} = 0$, and hence the Stefan equations at the two interfaces can be rewritten as:

$$\rho_l L_v \frac{\partial z_v}{\partial t} - k_l \frac{\partial T_l}{\partial z} = I_{abs} + \rho_l H_{ox} \eta_{ox} \frac{\partial z_m}{\partial t} - h_g (T_{l0} - T_g) \quad (7)$$

$$\rho_s L_m \frac{\partial z_m}{\partial t} = \left(k_s \frac{\partial T_s}{\partial z} - k_l \frac{\partial T_l}{\partial z} \right) \quad (8)$$

By looking at the actual drilled hole geometry, $z_m(r,t)$ and $z_v(r,t)$ may be assumed to have parabolic profiles, i.e.

$$z_m(r,t) = z_{m0}(t) - \frac{r^2}{r_{m0}^2} z_{m0}(t) \quad (9)$$

$$z_v(r,t) = z_{v0}(t) - \frac{r^2}{r_{v0}^2} z_{v0}(t) \quad (10)$$

where $z_{m0}(t)$ and $z_{v0}(t)$ are the melt depth and vaporization depth at $r = 0$ and r_{m0} is the radius of the solid-liquid interface at the hole entrance, respectively.

By substituting Eq.(9) and (10) into Eq.(7) and (8), Stefan conditions at the two interfaces can be written as:

$$\rho_l L_v \frac{dz_{v0}(t)}{dt} - k_l \frac{T_m - T_{l0}}{z_{m0}(t) - z_{v0}(t)} = I_{abs} + \rho_l H_{ox} \eta_{ox} \frac{dz_{m0}(t)}{dt} - h_g (T_{l0} - T_g) \quad (11)$$

$$\rho_s L_m \frac{dz_{m0}(t)}{dt} = k_s \frac{(T_m / e) - T_m}{2\sqrt{\alpha_s t}} - k_l \frac{T_m - T_{l0}}{z_{m0}(t) - z_{v0}(t)} \quad (12)$$

where α_s is the thermal diffusivity of solid.

Combining Eqs.(11) and (12) gives,

$$z'_{v0}(t) = \frac{1}{\rho_l L_v} [I_{abs} + h_g (T_g - T_{l0}) + \frac{k_s T_m (\frac{1}{e} - 1)}{2\sqrt{\alpha_s t}} + \rho_l H_{ox} \eta_{ox} z'_{m0}(t) + \rho_s L_m z'_{m0}(t)] \quad (13)$$

where $z'_{v0}(t) = \frac{dz_{v0}(t)}{dt}$ and $z'_{m0}(t) = \frac{dz_{m0}(t)}{dt}$.

2.2 Mass balance

As the drilling occurs mainly in the vertical direction, it is possible to assume that the mass of the solid melt at the solid-liquid interface is equal to the mass removed due to melt ejection and vaporization, i.e.

$$S_{sl} \rho_s \frac{\partial z_m}{\partial t} = S_m \rho_l V_m + S_{lv} \rho_l \frac{\partial z_v}{\partial t} \quad (14)$$

where S_{sl}, S_{lv}, S_m, and V_m are the solid-liquid interface area, liquid-vapour interface area, melt ejection area, and the melt ejection velocity, respectively.

For parabolic hole profile, the surface area S_{sl} and S_{lv} are estimated by:

$$S_{sl} = \frac{\pi r_{m0}}{6z_{m0}^2(t)}[(r_{m0}^2 + 4z_{m0}^2(t))^{3/2} - r_{m0}^3] \qquad (15)$$

$$S_{lv} = \frac{\pi r_{v0}}{6z_{v0}^2(t)}[(r_{v0}^2 + 4z_{v0}^2(t))^{3/2} - r_{v0}^3] \qquad (16)$$

Eq.(14) can now be expressed as:

$$\frac{\pi r_{m0}}{6z_{m0}^2(t)}[(r_{m0}^2 + 4z_{m0}^2(t))^{3/2} - r_{m0}^3]\rho_s\left(z'_{m0}(t) - \frac{r^2 z'_{m0}(t)}{r_{m0}^2}\right) = \pi(r_{m0}^2 - r_{v0}^2)\rho_l V_m + \frac{\pi r_{v0}}{6z_{v0}^2(t)}[(r_{v0}^2 + 4z_{v0}^2(t))^{3/2} - r_{v0}^3]\times \rho_l\left(z'_{v0}(t) - \frac{r^2 z'_{v0}(t)}{r_{v0}^2}\right) \qquad (17)$$

As $r \to 0$, the mass equation becomes:

$$\frac{\pi r_{m0}}{6z_{m0}^2(t)}[(r_{m0}^2 + 4z_{m0}^2(t))^{3/2} - r_{m0}^3]\rho_s z'_{m0}(t) = \pi(r_{m0}^2 - r_{v0}^2)\rho_l V_m + \frac{\pi r_{v0}}{6z_{v0}^2(t)}[(r_{v0}^2 + 4z_{v0}^2(t))^{3/2} - r_{v0}^3]\ \rho_l z'_{v0}(t) \qquad (18)$$

However, because Eq.(18) is quite complex, solving the system of equations analytically would be a time consuming process. Therefore, for the sake of simplicity, the paraboloid surface area is approximated here by the conical surface area, which can be formulated in a much simpler form. Collins [11] has also developed a model using both conical and parabolic profiles. The results confirm that there is no significant difference in the hole depth prediction.

The mass balance can now be expressed in term of the conical surface area as:

$$sc\, r_{m0}\rho_s z'_{m0}(t)\sqrt{r_{m0}^2 + t^2(z'_{m0}(t))^2} = (r_{m0}^2 - r_{v0}^2)\rho_l V_m + sc\, r_{v0}\rho_l z'_{v0}(t)\sqrt{r_{v0}^2 + t^2(z'_{v0}(t))^2} \qquad (19)$$

where sc is a surface area correction factor and is taken to be 1.23 in this model. Eq.(19) may be rearranged as:

$$z'_{v0}(t) = \frac{1}{\sqrt{2}}\sqrt{\frac{-r_{v0}^4 sc^2\rho_l^2 + \sqrt{r_{v0}^2 sc^2\rho_l^2(a_1 + a_2 + a_3)}}{r_{v0}^2 sc^2 t^2\rho_l^2}} \qquad (20)$$

where

$$a_1 = (r_{v0}^6 sc^2 + 4r_{m0}^4 t^2 V_m^2 - 8r_{m0}^2 r_{v0}^2 t^2 V_m^2 + 4r_{v0}^2 t^2 V_m^2)\rho_l^2$$

$$a_2 = 4r_{m0}^4 sc^2 t^2\rho_s^2(z'_{m0}(t))^2 + 4r_{m0}^2 sc^2 t^4\rho_s^2(z'_{m0}(t))^4,$$

$$a_3 = 8r_{m0}(-r_{m0}^2 + r_{v0}^2)sc\, t^2 V_m\rho_l\rho_s z'_{m0}(t)\times \sqrt{r_{m0}^2 + t^2(z'_{m0}(t))^2}$$

By equating (13) to (20), $z'_{m0}(t)$ and $z'_{v0}(t)$ can now be determined.

The positions of the solid-liquid and liquid-vapour interfaces at $r = 0$ can be determined from:

$$z_{m0}(t) = \int_0^t z'_{m0}(t)dt \quad (21)$$

$$z_{v0}(t) = \int_0^t z'_{v0}(t)dt \quad (22)$$

2.3 Melt front radius at the hole entrance

In laser drilling of metals, the hole entrance diameter is usually larger than the theoretical beam spot diameter due to radial heat diffusion. Hence, the hole entrance diameter is estimated from [12]:

$$T_r(r,t)=\frac{P_p}{2\pi\alpha_l\rho_l c_{pl}t}\exp\left(\frac{-r^2}{4\alpha_l t}\right) \quad (23)$$

where T_r and P_p are temperature distribution in the radial direction and laser peak power. The melt front radius at the hole entrance (r_{m0}) is hence approximated by a radial distance at which $T_r = T_m$.

2.4 Melt ejection velocity

From Eq.(20), value of the melt ejection velocity is required. It may be determined by using Bernoulli's equation:

$$p_{vap} + p_{eff} = \frac{\rho_l V_m^2}{2} + \rho_l g z_{m0}(t) + \frac{\sigma}{r_b} \quad (24)$$

where p_{vap}, p_{eff}, g and σ are vapour pressure, effective assist gas pressure, gravitational acceleration and surface tension, respectively. Hence, the melt front velocity is written as:

$$V_m = \sqrt{\frac{2\,(p_{vap} + p_{eff})}{2\,\rho_l}} \quad (25)$$

2.5 Vapour pressure

Vapour pressure exerted on the melt surface can be estimated from the Clausius-Clapeyron equation [13]:

$$p_{vap} = p_0 \exp\left[\frac{L_v}{R}\left(\frac{1}{T_b} - \frac{1}{T_{l0}}\right)\right] \quad (26)$$

where p_0 and T_b are atmospheric pressure and boiling temperature, R is the specific gas constant.

2.6 Effective assist gas pressure

For isentropic gas flow, total pressure, which consists of static and dynamic pressure terms, is constant along the gas stream. However, in a case of laser drilling, where the hole bottom is perpendicular to the gas axis, and if a uniform gas pressure profile is assumed within the laser beam, the dynamic gas pressure may be negligible. Due to adiabatic expansion of the assist gas at the nozzle exit, the gas is accelerated up to the local speed of sound leading to the critical state [8-9]. The critical assist gas pressure at the nozzle exit, p_c, can be defined as:

$$p_c = \left(\frac{2}{\gamma+1}\right)^{\frac{\gamma}{\gamma-1}} p_i \quad (27)$$

where p_i is the pressure inside the nozzle, γ is the specific heat ratio which is taken to be 1.4 for oxygen.

At the hole entrance, assist gas pressure is reduced from p_c to p_{eff} due to pressure loss between the gas nozzle exit and the hole entrance.

$$p_{eff} = p_c \frac{A_{eff}}{A_{eff} + A_{rl}} \quad (28)$$

where $$A_{eff} = \pi r_b^2 \quad (29)$$

$$A_{rl} = \pi d_n z_n \quad (30)$$

The mathematical model developed above consists of mostly non-linear equations. The solutions of the model which give relationship amongst various parameters can be obtained by taking the following calculation procedures.

1) Assume a melt surface temperature.

2) Calculate the vapour pressure from Eq. (26).

3) Calculate the assist gas pressure from Eq. (28).

4) Calculate the melt ejection velocity from Eq. (25).

5) Calculate the melt front velocity and the vapour front velocity at $r = 0$ from Eq. (13) and Eq. (20).

6) Calculate the locations of the melt front and vapour front from Eq. (21) and Eq. (22).

3. Physical Properties

The thermophysical properties of the low carbon steel and assist gas are given as in Tables 1 and 2.

4. Results and Discussion

In this section, the predicted results are reported and discussed. In this present model, the melt surface temperature T_{l0} is assumed to be from slightly above the boiling point up to some point around 5,000 K. Comparison with the experiment reveals that T_{l0} = 4,000 K seems to be the most compromising option for mild steel. Therefore, this value is employed throughout the modelling work presented here. Fig. 2 shows the comparison between the measured hole depth and the calculated value for laser drilling of mild steel. It can be seen that the model gives good agreement with the experimental data.

Fig. 3 shows the evolution of hole depth as a function of number of pulses for the cases of 1.0 and 1.5 ms pulse width. To investigate the pulse width effects, laser beam-material interaction time t is increased unitl t = pulse width. This is followed by the pulse off period where no interaction takes place. At the end of the pulse off time, the subsequent laser pulse is delivered to the workpiece and the process repeats. It can be seen from Fig. 3 that the hole depth increases sharply during the interaction with the first laser pulse. The subsequent laser pulses propagate into the workpiece at an approximately constant speed. The recession of the drilling speed can be attributed to the fact that once the cavity is produced, vapour formed above the liquid surface may absorb and block part of laser energy resulting in beam scattering and causing less energy being delivered to the workpiece, hence lowering drilling rate. Fig. 3 also shows that the longer pulse width produces the deeper hole. This is because

the longer laser pulse width delivers more laser energy to the workpiece.

Fig. 4 illustrates the predicted profiles of solid-liquid and liquid-vapour interfaces after interacting with 1 and 2 pulses. The hole profiles plotted in this figure are for the case of blind holes. It can be seen that once a keyhole has been produce by the first pulse, subsequent laser pulses enlarge the hole wall, hence resulting in smaller hole taper.

In Fig. 5, number of pulses required to initiate the breakthrough are plotted at various peak power values. At high peak power, more laser energy is absorbed by the workpiece resulting in higher penetration rate. Therefore, less pulse is required to produce a through hole.

Fig. 6 shows the hole depth evolutions calculated using 3, 4, and 5 bar of assist gas pressure in the model. It can be seen that assist gas pressure alone has no significant impact on the melt depth. Calculations show that oxygen assist gas has more pronounced effects on producing exothermic energy to the process rather than adding the pressure to the recoil pressure.

5. Conclusion

This paper presents a mathematical model of laser percussion drilling incorporating the effects of: (i) exothermic reaction, (ii) assist gas pressure, and (iii) recoil pressure into the model. Assuming that the solid-liquid and liquid-vapour interfaces have parabolic profiles, the model enables the prediction of the hole depth and hole profile. The results obtained from the model show that:

1. The drilling rate rises sharply in the beginning and becomes slower as the number of laser pulses increase. Subsequent laser pulses, however, play a more important role in enlarging the hole at the exit.
2. The increase in pulse width and peak power results in a deeper hole.
3. Assist gas pressure has no significant influence on the hole depth.

6. Reference

[1] J. J. Benes, “Technology Adds a New Twist to Difficult Drilling”, American Mechinist 140, 1996, pp. 78-79.

[2] L. Li, “The Challenges ahead for Laser Macro, Micro, and Nano Manufacturing”, In: J. Lawrence, J. Pou, D.K.Y. Low, and E.Toyserkani (Ed.) “Advances in Laser Materials Processing: Technology, Research and Applications”, CRC Press, Oxford. 2010.

[3] R.S.Patel and M.Q.Brewster, “Gas-Assisted Laser-Metal Drilling: Theoretical Model”, Journal of Thermophysics and Heat Transfer 5, 1991, pp. 32-39.

[4] S. Sankaranarayanan, H. Emminger, and A. Kar, “Energy Loss in the Plasma during Laser Drilling”, Journal of Physics D: Applied Physics 32, 1999, pp. 1605-1611.

[5] M.F. Modest, "Effects of Multiple Reflections on Hole Formation During Short-Pulsed Laser Drilling", Journal of Heat Transfer 128, 2006, pp. 653-661.

[6] M.V. Allmen, "Laser Drilling Velocity in Metals", Journal of Applied Physics 47, 1976, pp. 5460-5463.

[7] A.Kar and J.Mazumder, "Two-Dimensional Model for Material Damage due to Melting and Vaporization during Laser Irradiation", Journal of Applied Physics 68, 1990, pp. 3884-3891.

[8] G.K.L. Ng, P.L. Crouse, and L. Li, "An Analytical Model for Laser Drilling Incorporating Effects of Exothermic Reaction, Pulse Width and Hole Geometry", International Journal of Heat and Mass Transfer 49, 2006, pp. 1358-1374.

[9] D.K.Y. Low, L. Li, and P.J. Byrd, "Hydrodynamic Physical Modeling of Laser Drilling", Transactions of the ASME 124, 2002, pp. 852-862.

[10] R.E.Wagner, "Laser Drilling Mechanics", Journal of Applied Physics 45, 1974, pp. 4631-4637.

[11] J. Collins and P. Gremaud, "A Simple Model for Laser Drilling", Mathematics and Computers in Simulation 81, 2011, pp. 1541-1552.

[12] H.S. Carslaw and J.C. Jaeger, "*Conduction of Heat in Solids"*, Oxford University Press, Newyork. 1959.

[13] D.A. McQuarrie and J.D. Simon, "*Physical Chemistry - A Molucular Approach"*, University Science Books, Sausalito, Calif. 1997.

[14] V. Semak and A.Matsunawa, "The Role of Recoil Pressure in Energy Balance during Laser Materials Processing", Journal of Physics D: Applied Physics 30, 1997, pp. 2541-2552.

[15] Y.S.Toulokian, P.E.Liley, and S.C.Saxena, "Thermophysical Properties of Matter: Thermal Conductivity", In: Y.S.Touloukian and C.Y.Ho (Ed.) "Thermophysical Properties of Matter vol. 3", IFI/Plenum, New York. 1970.

[16] Y.S.Toulokian, S.C.Saxena, and P.Hestermans, "Thermophysical Properties of Matter: Viscosity", In: Y.S.Touloukian and C.Y.Ho (Ed.) "Thermophysical Properties of Matter vol. 11", IFI/Plenum, New York. 1970.

[17] P.E.Liley, "*Properties of Nonmetallic Fluid Elements, McGraw-Hill/CINDAS Data Series on Material Properties* vol. III-2", McGraw-Hill, New York. 1981.

List of Tables

Table 1 Thermophysical properties of low carbon steel [14]

Physical properties	
Density of solid, ρ_s (kg m^{-3})	7800
Density of liquid, ρ_l (kg m^{-3})	6980
Specific heat of solid, c_{ps} (J kg^{-1} K^{-1})	628
Specific heat of liquid, c_{pl} (J kg^{-1} K^{-1})	748
Thermal diffusivity of solid, α_s (m^2 s^{-1})	0.014×10^{-3}
Thermal diffusivity of liquid, α_l (m^2 s^{-1})	0.007×10^{-3}
Latent heat of melting, L_m (J kg^{-1})	276×10^3
Latent heat of vaporization, L_v (J kg^{-1})	6088×10^3
Initial temperature, T_0 (K)	300
Melting temperature, T_m (K)	1808
Boiling temperature, T_b (K)	3100

Table 2 Thermophysical properties of O_2 assist gas [15-17] and gas nozzle parameters

O_2 properties	
Density of gas, ρ_g (kg m^{-3})	1.3007
Viscosity of gas, μ_g (N s m^{-2})	2.01×10^{-5}
Thermal conductivity, k_g (W m^{-1}K^{-1})	0.0259
Prandtl number, Pr	0.73
Assist gas nozzle exit diameter, d_n (m^2)	1.5×10^{-3}
Nozzle-workpiece distance, z_n (m)	5.8×10^{-3}

List of Figures

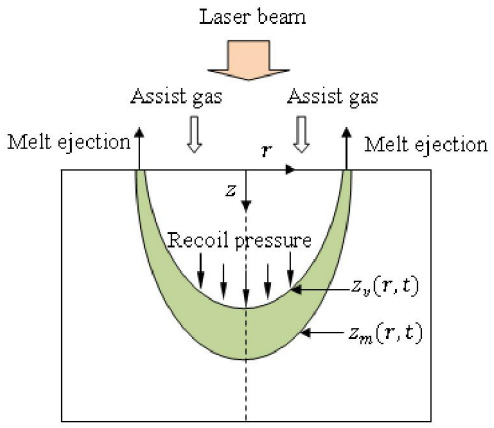

(a)

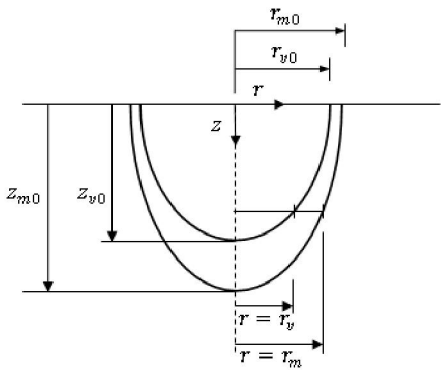

(b)

Fig. 1. (a) schematic diagram of the model, (b) variables defined in the model.

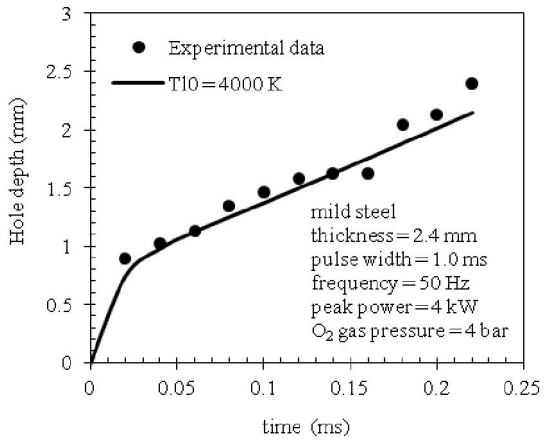

Fig. 2. Comparison between the predicted and measured hole depth

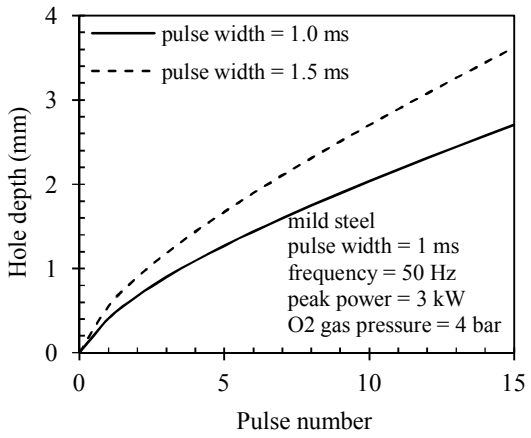

Fig. 3. Hole depth prediction

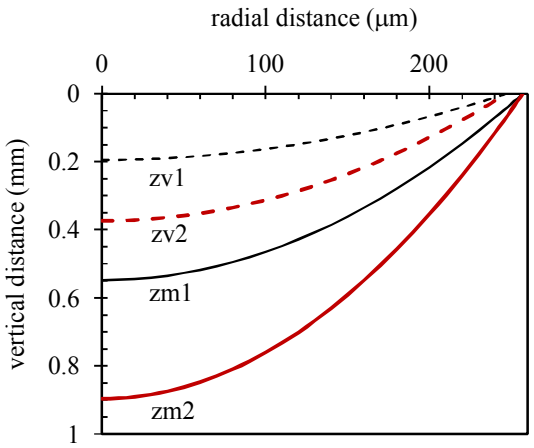

Fig. 4. Hole profiles

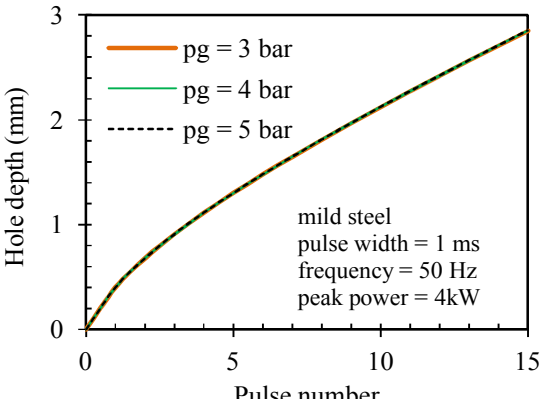

Fig. 6. Effects of assist gas pressure on melt depth

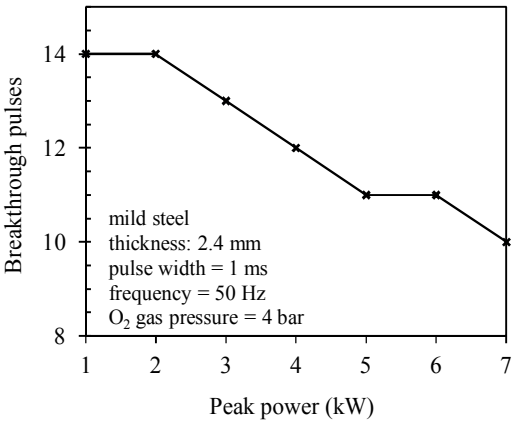

Fig. 5. Effects of peak power on breakthrough pulses